Geophys. J. Int. (2009) **176,** 938–950 doi: 10.1111/j.1365-246X.2008.04026.x

Scattering of plane transverse waves by spherical inclusions in a poroelastic medium

Xu Liu,[1] Stewart Greenhalgh[1,2] and Bing Zhou[1]

[1]*Department of Physics, University of Adelaide, North Terrace Campus, Adelaide* SA 5005, *Australia. E-mail: xu.liu@adelaide.edu.au*
[2]*Institute of Geophysics, ETH Zürich, Hönggerberg,* 8093 CH *Switzerland*

Accepted 2008 October 20. Received 2008 October 19; in original form 2008 April 28

SUMMARY

The scattering of plane transverse waves by a spherical inclusion embedded in an infinite poroelastic medium is treated for the first time in this paper. The vector displacement wave equations of Biot's theory are solved as an infinite series of vector spherical harmonics for the case of a plane *S*-wave impinging from a porous medium onto a spherical inclusion which itself is assumed to be another porous medium. Based on the single spherical scattering theory and dynamic composite elastic medium theory, the non-self-consistent shear wavenumber is derived for a porous rock having numerous spherical inclusions of another medium. The frequency dependences of the shear wave velocity and the shear wave attenuation have been calculated for both the patchy saturation model (inclusions having the same solid frame as the host but with a different pore fluid from the host medium) and the double porosity model (inclusions having a different solid frame than the host but the same pore fluid as the host medium) with dilute concentrations of identical inclusions. Unlike the case of incident *P*-wave scattering, we show that although the fluid and the heterogeneity of the rock determine the shear wave velocity of the composite, the attenuation of the shear wave caused by scattering is actually contributed by the heterogeneity of the rock for spherical inclusions. The scattering of incident shear waves in the patchy saturation model is quite different from that of the double porosity model. For the patchy saturation model, the gas inclusions do not significantly affect the shear wave dispersion characteristic of the water-filled host medium. However, the softer inclusion with higher porosity in the double porosity model can cause significant shear wave scattering attenuation which occurs at a frequency at which the wavelength of the shear wave is approximately equal to the characteristic size of the inclusion and depends on the volume fraction. Compared with analytic formulae for the low frequency limit of the shear velocity, our scattering model yields discrepancies within 4.0 per cent. All calculated shear velocities of the composite medium with dilute inclusion concentrations approach the high frequency limit of the host material.

Key words: Microstructure; Permeability and porosity; Seismic attenuation; Wave scattering and diffraction; Acoustic properties.

1 INTRODUCTION

The scattering of elastic waves in heterogeneous media has been considered for well over a century, with studies dating back to 1863 (see Waterman 1976). The subject finds important application in a variety of fields, including non-destructive material testing, seismic exploration, mechanical properties of composite materials and questions of dynamic stress concentration.

The scattering by a single inclusion has proven to be significant for studies of wave attenuation and determination of effective constants for elastic and poroelastic composite materials. The scattering in a porous medium has been well researched. Berryman (1985) first analysed the scattering from a porous spherical inclusion in an otherwise homogeneous porous host medium. One major difficulty is that the solution is given in terms of an infinite series, and one needs to solve a 6×6 system of equations for the coefficients at each harmonic. The analytical solution can be obtained only after some simplifications (Berryman 1985; Zimmerman & Stern 1993, 1994; Morochnik & Bardet 1996; Ciz & Gurevich 2005). Kargl & Lim (1993) used a transition matrix approach to numerically solve for the wave scattered from a porous obstacle of arbitrary shape. This approach provides a general solution which allows the incident wave to be longitudinal or transverse. However, the coefficients of the expanded harmonics are expressed in the form of surface integrals which are more suitable for numerical calculation.

Ciz *et al.* (2006) and Markov & Levin (2007) applied Waterman–Truell multiple scattering theory to relate the scattering of a single obstacle to the wave attenuation in the medium.

The White model, also referred to as the patchy saturation model, requires the presence of gas-filled zones in water-saturated porous media and predicts high attenuation in a porous sedimentary rock over the seismic frequency band (White 1975; Dutta & Odé 1979a,b). In this model, a small amount of gas in a fluid-saturated porous medium can significantly affect the velocity and the attenuation of the *P* wave. From the scattering point of view, incident *P* waves can be strongly reflected by a gas–water interface in porous media and the Biot slow *P* waves are excited around the gas–water interface of the spherical surface with the same solid frame on both sides. As pointed out by Müller & Gurevich (2005), the processes of wave conversion scattering is equivalent to the mechanism of pore pressure relaxation due to wave-induced perturbation and thus also describes the mechanism of wave-induced fluid flow. This is the reason why partially gas saturated media can be highly attenuating.

All of the above papers consider the incident wave to be a compressional (longitudinal) wave. However, it is difficult to extend the White model to shear waves to get a complex frequency-dependent shear modulus in the same way at low frequencies. The problem is that the fluid filling the pores does not change the shear force which exists in the solid frame, nor the shear modulus, and so a small amount of gas has almost no effect on the velocity of shear waves.

Pride *et al.* (2004) show that the patchy saturation model has similar attenuation behaviour to the double porosity model (two different porous frames) for acoustic (*P*) waves. However, in natural hydrocarbon reservoirs and surrounding rocks, *P*-wave attenuation can be caused by either of the two models, or by gas in the reservoir and by heterogeneity of the rock. A logical question to ask is which model dominates the *P*-wave dispersion. It is also logical and important to investigate the similarity between the partially saturated model and double porosity model for incident shear waves. There are three main attenuation mechanisms which have been proposed: (1) *S*-wave to *S*-wave and *S*-wave to *P*-wave scattering and resonance for shear wavelengths of approximately the inclusion diameter; (2) Biot relaxation or Biot global flow at the relaxation frequency of the host medium; (3) *S*-wave to slow *P*-wave scattering or attenuation due to wave-induced flow of the pore fluid. We believe that elucidation of the difference between the patchy saturation model and the double porosity model will provide more information about porous soils and rocks. A complication for an incident shear wave, as opposed to a longitudinal wave, is that the wavefields are not azimuthally symmetric. The polarization of the incident wave causes the wavefields to be dependent on the azimuth angle. The vector Helmholtz equation must therefore be solved in this case (Morse & Feshbach 1953).

Some papers (Einspruch *et al.* 1960; Lim & Hackman 1990; Korneev & Johnson 1993, 1996) have considered *S*-wave scattering in purely elastic media but no theoretical solutions have yet been given for poroelastic media. However, numerical (finite difference) modelling in such media was undertaken by Masson & Pride (2007). They determined shear attenuation by scattering from a soft porous ellipsoid embedded within a stiffer matrix. They showed that significant attenuation occurs over the seismic frequency range. Some experiments (Jones 1986) show that the inverse quality factor ($1/Q(\omega)$) of shear waves could be of a similar magnitude to that of compressional waves in fluid-saturated porous media, and so a model needs to be developed to predict the frequency-dependent shear velocity and attenuation because both of them are measurable.

To the best of our knowledge, none has considered a series solution for the scattering by an incident shear wave in poroelastic media, so this is a promising line of research to pursue. In this paper, we develop the basic equations for *S*-wave scattering in a poroelastic medium and present phase velocities and attenuation characteristics for various poroelastic materials with different spherical inclusion concentrations. Since the sphere is one of several popular and simple geometric inclusions, and is also a special case of the ellipsoid, our incident shear wave scattering solution provides a discernible contrast with the incident compressional wave case and a basic reference against which to test the analytical solution for ellipsoidal inclusions.

2 VECTOR WAVE EQUATIONS OF BIOT'S THEORY

For a harmonic wave with $\exp(-\mathrm{i}\omega t)$ time dependence, the vector wave equations of Biot's theory (Biot 1962) can be written as

$$(\lambda_c + \mu)\nabla\nabla\cdot\mathbf{u} + \mu\nabla^2\mathbf{u} + \alpha M\nabla\nabla\cdot\mathbf{w} + \omega^2(\rho\mathbf{u} + \rho_f\mathbf{w}) = 0, \tag{1}$$

$$\alpha M\nabla\nabla\cdot\mathbf{u} + M\nabla\nabla\cdot\mathbf{w} + \omega^2(\rho_f\mathbf{u} + q(\omega)\mathbf{w}) = 0, \tag{2}$$

where $\mathbf{u}$ is the displacement of the solid frame of components u_i, $\mathbf{w}$ is the displacement of the fluid relative to the solid components (measured in volume per unit area) which can be related to the displacement of the fluid $\mathbf{U}$ and the porosity β by $\mathbf{w} = \beta(\mathbf{U} - \mathbf{u})$, μ is the shear modulus ρ_f and ρ are the density of the pore fluid and the average density of the rock. The coefficients α and M are given by Brown & Korringa (1975) and Berryman & Milton (1991) as $\alpha = 1 - K_m/K_s$, $1/M = \alpha/K_s + \phi(1/K_f - 1/K_s)$, where K_m, K_s and K_f, are the bulk moduli of the porous frame, the grain and the pore fluid respectively. According to Biot (1962) λ_c can be expressed as $\lambda_c = K_m - 2\mu/3 + \alpha^2 M$. The operator $q(\omega)$ is called the frequency dynamic operator and can be expressed as

$$q(\omega) = \frac{\mathrm{i}\eta}{\omega\kappa(\omega)}, \tag{3}$$

where η is viscosity of the pore fluid and $\kappa(\omega)$ is the dynamic permeability.

The dynamic permeability $\kappa(\omega)$ can also be viewed as static permeability κ_0 multiplied by its frequency correction factor (Johnson *et al.* 1987),

$$\kappa(\omega) = \kappa_0 \left[\sqrt{1 - \mathrm{i}\frac{4\omega}{n_\mathrm{J}\omega_\mathrm{t}}} - \mathrm{i}\frac{\omega}{\omega_\mathrm{t}} \right]^{-1}. \tag{4}$$

Here, the frequency ω_t is called the transition frequency or relaxation frequency (Pride *et al.* 2004) which separates the viscous-force-dominated flow from the inertial-force-dominated flow. It is given by

$$\omega_\mathrm{t} = \eta/(\rho_\mathrm{f} F \kappa_0). \tag{5}$$

The quantity $n_\mathrm{J} = \Lambda^2/\kappa_0 F$, where Λ represents the pore volume-to-surface ratio and has the dimensions of length. F is the electric formation factor and it can also be related to the tortuosity α_∞ and porosity β through the relation: $F = \alpha_\infty \beta^{-1}$.

Dutta & Odé (1979a,b) decoupled the two equations in the low frequency range. Following their approach, we decouple equations of (1) and (2) into three vector Helmholtz equations for the fluid displacement as

$$\left(\nabla^2 + k_s^2\right)\mathbf{w}_s = 0, \tag{6}$$

$$\left(\nabla^2 + k_c^2\right)\mathbf{w}_c = 0, \tag{7}$$

$$\left(\nabla^2 + k_d^2\right)\mathbf{w}_d = 0. \tag{8}$$

The linear relationships between the displacements of the solid frame and those of the fluid relative to the solid frame are

$$\mathbf{w}_s = A_s \mathbf{u}_s, \quad \mathbf{w}_c = A_c \mathbf{u}_c, \quad \mathbf{w}_d = A_d \mathbf{u}_d. \tag{9}$$

Here, k_s, k_c and k_d are the complex wavenumbers of the shear wave, the fast P wave and the slow P wave, respectively. These values and the relative fluid displacement coefficients A_s, A_c and A_d can be calculated from material parameters (see Appendix A).

The three vector Helmholtz wave equations (6–8) and the linear relationships (9), along with the boundary conditions for porous media (Deresiewicz & Skalak 1963) provide a basis for formulating wave propagation in porous media.

3 FIELD EXPANSIONS BY VECTOR SPHERICAL HARMONICS

Waves propagated in a porous medium may be expanded in a complete basis formed from the eigenfunctions of the vector Helmholtz equation expressed in a separable coordinate system. In spherical coordinates (r, θ, ϕ), an applicable set of normalized vector eigenfunctions $\psi_{\tau\sigma mn}$ can be written as (Morse & Feshbach 1953; Kargl & Lim 1993)

$$\psi_{1\sigma mn} = F_c^{-1}\left\{ h_n'(k_c r)\mathbf{A}_{\sigma mn}(\theta,\phi) + \xi_n^{1/2}[h_n(k_c r)/k_c r]\mathbf{B}_{\sigma mn}(\theta,\phi)\right\}, \tag{10}$$

$$\psi_{2\sigma mn} = F_d^{-1}\left\{ h_n'(k_d r)\mathbf{A}_{\sigma mn}(\theta,\phi) + \xi_n^{1/2}[h_n(k_d r)/k_d r]\mathbf{B}_{\sigma mn}(\theta,\phi)\right\}, \tag{11}$$

$$\psi_{3\sigma mn} = h_n(k_s r)\mathbf{C}_{\sigma mn}(\theta,\phi), \tag{12}$$

$$\psi_{4\sigma mn} = \xi_n^{1/2}[h_n(k_s r)/k_s r]\mathbf{A}_{\sigma mn}(\theta,\phi) + [h_n'(k_s r) + h_n(k_s r)/k_s r]\mathbf{B}_{\sigma mn}(\theta,\phi), \tag{13}$$

where $\xi_n = n^2 + n$ and $F_\tau = [(k_s/k_\tau)(P + 2QA_\tau + RA_\tau^2)/\mu]^{1/2}$, $(\tau = c, d)$. By comparing the wave equations given by Kargl & Lim (1993) with those of Biot (1962), we have $P = \lambda_\mathrm{c} + 2\mu + (\beta - 2\alpha)\beta M$, $Q = (\alpha - \beta)\beta M$ and $R = \beta^2 M$. F_τ are the factors used by Kargl & Lim (1993) to normalize the basis function so that the time-averaged energy per unit time per unit area crossing a surface enclosing the origin is $\omega\mu/2k_s$. Although we keep the normalization factors F_τ in the following derivation, they can be any non-zero constants for the solutions because the factors can be included in the unknown coefficients of the expanded vector series (to be shown in following sections). A mode index τ in the wavefunctions $\psi_{\tau\sigma mn}$, which takes the values $\tau = 1, 2, 3, 4$, is used above to indicate the spherical modes of the classic (fast) P wave, the slow P wave and the two mutually perpendicular shear waves, having respective wavenumbers k_c, k_d for $\tau = 1, 2$ and k_s for $\tau = 3, 4$. The terms σ, m and n are the indices of the spherical harmonics. The quantity $\sigma(= e,\ a)$ specifies azimuthal parity; $n(= 0, 1, 2 \cdots \infty)$ specifies order, but there is no zero order for the shear waves; $m(\leq n)$ specifies the rank of the spherical harmonics. Spherical Hankel functions of the first kind are denoted by h_n and a prime on this quantity indicates differentiation with respect to the argument. $\mathbf{A}_{\sigma mn}(\theta,\phi)$, $\mathbf{B}_{\sigma mn}(\theta,\phi)$ and $\mathbf{C}_{\sigma mn}(\theta,\phi)$ are vector spherical harmonics which are the functions of spherical surface harmonic Y_{mn}^{σ} (see Morse and Feshbach 1953; Kargl & Lim 1993 for details). Their explicit form is given in Appendix B.

The vector spherical harmonics satisfy the orthogonality conditions:

$$\mathbf{A}_{\sigma mn}\cdot\mathbf{B}_{\sigma mn} = \mathbf{A}_{\sigma mn}\cdot\mathbf{C}_{\sigma mn} = \mathbf{B}_{\sigma mn}\cdot\mathbf{C}_{\sigma mn} = 0, \tag{14}$$

$$\int_{4\pi}\mathbf{A}_{\sigma mn}\cdot\mathbf{A}_{vpq}\,\mathrm{d}S = \int_{4\pi}\mathbf{B}_{\sigma mn}\cdot\mathbf{B}_{vpq}\,\mathrm{d}S = \int_{4\pi}\mathbf{C}_{\sigma mn}\cdot\mathbf{C}_{vpq}\,\mathrm{d}S = \delta_{\sigma v}\delta_{mp}\delta_{nq}. \tag{15}$$

Here, integration is performed over the surface of a unit sphere ($\mathrm{d}S = \sin\theta\,\mathrm{d}\theta\,\mathrm{d}\phi$).

To apply the spherical boundary conditions, it is more convenient to express wavefields according to the components of the vector spherical harmonics. So, we rewrite eqs (10)–(13) as

$$\psi_{1\sigma mn} = u_{1An}\mathbf{A}_{\sigma mn}(\theta,\phi) + u_{1Bn}\mathbf{B}_{\sigma mn}(\theta,\phi), \tag{16}$$

$$\psi_{2\sigma mn} = u_{2An}\mathbf{A}_{\sigma mn}(\theta,\phi) + u_{2Bn}\mathbf{B}_{\sigma mn}(\theta,\phi), \tag{17}$$

$$\psi_{3\sigma mn} = u_{3Cn}\mathbf{C}_{\sigma mn}(\theta,\phi), \tag{18}$$

$$\psi_{4\sigma mn} = u_{4An}\mathbf{A}_{\sigma mn}(\theta,\phi) + u_{4Bn}\mathbf{B}_{\sigma mn}(\theta,\phi). \tag{19}$$

The radial frame traction vector $\mathbf{t}_r$ and the fluid traction vectors $p\hat{\mathbf{r}}$ of the normalized vector eigenfunctions can be determined by Biot's constitutive relations (see Kargl & Lim 1993).

$$\mathbf{t}_r(\psi_{1\sigma mn}, A_1\psi_{1\sigma mn}) = t_{1An}\mathbf{A}_{\sigma mn}(\theta,\phi) + t_{1Bn}\mathbf{B}_{\sigma mn}(\theta,\phi), \tag{20}$$

$$\mathbf{t}_r(\psi_{2\sigma mn}, A_2\psi_{2\sigma mn}) = t_{2An}\mathbf{A}_{\sigma mn}(\theta,\phi) + t_{2Bn}\mathbf{B}_{\sigma mn}(\theta,\phi), \tag{21}$$

$$\mathbf{t}_r(\psi_{3\sigma mn}, A_3\psi_{3\sigma mn}) = t_{3Cn}\mathbf{C}_{\sigma mn}(\theta,\phi), \tag{22}$$

$$\mathbf{t}_r(\psi_{4\sigma mn}, A_s\psi_{4\sigma mn}) = t_{4An}\mathbf{A}_{\sigma mn}(\theta,\phi) + t_{4Bn}\mathbf{B}_{\sigma mn}(\theta,\phi), \tag{23}$$

$$\beta p(\psi_{1\sigma mn}, A_1\psi_{1\sigma mn})\hat{\mathbf{r}} = p_{1An}\mathbf{A}_{\sigma mn}(\theta,\phi), \tag{24}$$

$$\beta p(\psi_{2\sigma mn}, A_2\psi_{2\sigma mn})\hat{\mathbf{r}} = p_{2An}\mathbf{A}_{\sigma mn}(\theta,\phi), \tag{25}$$

$$p(\psi_{3\sigma mn}, A_s\psi_{3\sigma mn}) = p(\psi_{4\sigma mn}, A_s\psi_{s\sigma mn}) = 0. \tag{26}$$

Here, the coefficients of the vector spherical harmonics (from eqs 16–26) are functions of the scatterer radius and the material parameters. They are listed in Appendix C.

4 INCIDENT, SCATTERED AND REFRACTED WAVES

The notations $\mathbf{u}_i$, $\mathbf{u}_s$, and $\mathbf{u}_f$ denote the frame displacements of the incident wave, the scattered wave in the background medium and the refracted (transmitted) wave within the inhomogeneity, respectively. Correspondingly, $\mathbf{w}_i$, $\mathbf{w}_s$ and $\mathbf{w}_f$ denote the relative fluid displacements.

For the sake of convenience, the overbar means that h_n in a quantity should be replaced by the spherical Bessel functions j_n and the subscript 'o' denotes the obstacle or scatterer.

According to the vector basis functions defined above and the linear relations (9), we have

$$\mathbf{u}_i = \sum_{\tau\sigma mn} a_{\tau\sigma mn}\bar{\psi}_{\tau\sigma mn}, \qquad \mathbf{w}_i = \sum_{\tau\sigma mn} A_\tau a_{\tau\sigma mn}\bar{\psi}_{\tau\sigma mn}, \qquad \text{(in the host)}, \tag{27}$$

$$\mathbf{u}_s = \sum_{\tau\sigma mn} c_{\tau\sigma mn}\psi_{\tau\sigma mn}, \qquad \mathbf{w}_s = \sum_{\tau\sigma mn} A_\tau c_{\tau\sigma mn}\psi_{\tau\sigma mn}, \qquad \text{(in the host)}, \tag{28}$$

$$\mathbf{u}_f = \sum_{\tau\sigma mn} f_{\tau\sigma mn}\bar{\psi}_{o\,\tau\sigma mn}, \qquad \mathbf{w}_f = \sum_{\tau\sigma mn} A_\tau f_{\tau\sigma mn}\bar{\psi}_{o\,\tau\sigma mn} \qquad \text{, (inside the inclusion)}, \tag{29}$$

where $\tau = 1, 2, 3, 4$. The coefficients $a_{\tau\sigma mn}$ of the incident waves are assumed to be known, and $c_{\tau\sigma mn}$ and $f_{\tau\sigma mn}$ are the unknown coefficients to be determined.

The frame and the corresponding fluid relative displacement vectors of the incident shear wave can, respectively, be expanded into (see Lim & Hackman 1990)

$$\mathbf{u}_i = \exp(\mathrm{i}k_s z)\hat{\mathbf{x}} = \sum_{1}^{\infty}[a_{3a1n}\bar{\psi}_{3a1n} + a_{4e1n}\bar{\psi}_{4e1n}], \tag{30}$$

$$\mathbf{w}_i = A_s\exp(\mathrm{i}k_s z)\hat{\mathbf{x}} = A_s\sum_{1}^{\infty}[a_{3a1n}\bar{\psi}_{3a1n} + a_{4e1n}\bar{\psi}_{4e1n}], \tag{31}$$

where

$$a_{3a1n} = -\mathrm{i}^n[2\pi(2n+1)]^{1/2}, \qquad a_{4e1n} = \mathrm{i}^{(n+1)}[2\pi(2n+1)]^{1/2}. \tag{32}$$

By application of eqs (18) and (19), eq. (30) can be written as

$$\mathbf{u}_i = \hat{\mathbf{x}}\exp(\mathrm{i}k_s z) = \sum_{n=1}^{\infty}(a_{3a1n}\bar{u}_{3Cn}\mathbf{C}_{a1n} + a_{4e1n}\bar{u}_{4An}\mathbf{A}_{e1n} + a_{4e1n}\bar{u}_{4Bn}\mathbf{B}_{e1n}). \tag{33}$$

In a similar fashion as was done above for the incident wave, the frame displacements of the scattered and refracted waves can be written in the following general form by inserting eqs (16)–(19) into eqs (28) and (29):

$$\mathbf{u}_s = \sum_{\sigma,m,n} \begin{pmatrix} c_{1\sigma mn} u_{1An} \mathbf{A}_{\sigma mn} + c_{1\sigma mn} u_{1Bn} \mathbf{B}_{\sigma mn} \\ + c_{2\sigma mn} u_{2An} \mathbf{A}_{\sigma mn} + c_{2\sigma mn} u_{2Bn} \mathbf{B}_{\sigma mn} \\ + c_{3\sigma mn} u_{3Cn} \mathbf{C}_{\sigma mn} \\ + c_{4\sigma mn} u_{4An} \mathbf{A}_{\sigma mn} + c_{4\sigma mn} u_{4Bn} \mathbf{B}_{\sigma mn} \end{pmatrix}, \tag{34}$$

$$\mathbf{u}_f = \sum_{\sigma,m,n} \begin{pmatrix} f_{1\sigma mn} \bar{u}_{o\,1An} \mathbf{A}_{\sigma mn} + f_{1\sigma mn} \bar{u}_{o\,1Bn} \mathbf{B}_{\sigma mn} \\ + f_{2\sigma mn} \bar{u}_{o\,2An} \mathbf{A}_{\sigma mn} + f_{2\sigma mn} \bar{u}_{o\,2Bn} \mathbf{B}_{\sigma mn} \\ + f_{3\sigma mn} \bar{u}_{o\,3Cn} \mathbf{C}_{\sigma mn} \\ + f_{4\sigma mn} \bar{u}_{o\,4An} \mathbf{A}_{\sigma mn} + f_{4\sigma mn} \bar{u}_{o\,4Bn} \mathbf{B}_{\sigma mn} \end{pmatrix}. \tag{35}$$

Since the total traction consists of both the frame and the fluid traction, we have the radial traction of the incident wave $\mathbf{t}_i$, the scattered wave $\mathbf{t}_s$ and the refracted wave $\mathbf{t}_f$ as (see eqs 20–26)

$$\mathbf{t}_i = \mathbf{t}_r(\mathbf{u}_i, \mathbf{w}_i) - \beta p(\mathbf{u}_i, \mathbf{w}_i)\hat{\mathbf{r}}, \tag{36}$$

$$\mathbf{t}_s = \mathbf{t}_r(\mathbf{u}_s, \mathbf{w}_s) - \beta p(\mathbf{u}_s, \mathbf{w}_s)\hat{\mathbf{r}}, \tag{37}$$

$$\mathbf{t}_f = \mathbf{t}_r(\mathbf{u}_f, \mathbf{w}_f) - \beta_o p(\mathbf{u}_f, \mathbf{w}_f)\hat{\mathbf{r}}. \tag{38}$$

The constitutive relations linking the stress to the deformation of the medium (Biot 1962) and eqs (20)–(26) are linear, so it is convenient to write the radial traction vectors of the incident, scattered and refracted waves according to the vector spherical harmonics.

For the incident wave, we have

$$\mathbf{t}_i = \mathbf{t}_r(\mathbf{u}_i, \mathbf{w}_i) = \sum_{n=1}^{\infty} (a_{3a1n} \bar{t}_{3Cn} \mathbf{C}_{a1n} + a_{4e1n} \bar{t}_{4An} \mathbf{A}_{e1n} + a_{4e1n} \bar{t}_{4Bn} \mathbf{B}_{e1n}) \tag{39}$$

and for the scattered and refracted waves in general form respectively

$$\mathbf{t}_s = \sum_{\sigma,m,n} \begin{pmatrix} c_{1\sigma mn}(t_{1An} - p_{1An}) \mathbf{A}_{\sigma mn} + c_{1\sigma mn} t_{1Bn} \mathbf{B}_{\sigma mn} \\ + c_{2\sigma mn}(t_{2An} - p_{2An}) \mathbf{A}_{\sigma mn} + c_{2\sigma mn} t_{2Bn} \mathbf{B}_{\sigma mn} \\ + c_{3\sigma mn} t_{3Cn} \mathbf{C}_{\sigma mn} \\ + c_{4\sigma mn} t_{4An} \mathbf{A}_{\sigma mn} + c_{4\sigma mn} t_{4Bn} \mathbf{B}_{\sigma mn} \end{pmatrix} \tag{40}$$

$$\mathbf{t}_f = \sum_{\sigma,m,n} \begin{pmatrix} f_{1\sigma mn}(\bar{t}_{o\,1An} - \bar{p}_{o\,1An}) \mathbf{A}_{\sigma mn} + f_{1\sigma mn} \bar{t}_{o\,1Bn} \mathbf{B}_{\sigma mn} \\ + f_{2\sigma mn}(\bar{t}_{o\,2An} - \bar{p}_{o\,2An}) \mathbf{A}_{\sigma mn} + f_{2\sigma mn} \bar{t}_{o\,2Bn} \mathbf{B}_{\sigma mn} \\ + f_{3\sigma mn} \bar{t}_{o\,3Cn} \mathbf{C}_{\sigma mn} \\ + f_{4\sigma mn} \bar{t}_{o\,4An} \mathbf{A}_{\sigma mn} + f_{4\sigma mn} \bar{t}_{o\,4Bn} \mathbf{B}_{\sigma mn} \end{pmatrix}. \tag{41}$$

Here, the subscript 'o' refers to the material parameters inside the inclusion, that is, the obstacle or scatterer.

5 SOLUTION FOR A SPHERICAL POROUS INCLUSION

The problem in which the scattering inclusion is a homogeneous isotropic poroelastic sphere of poroelastic properties different from those of the infinite host in which the scatterer is embedded will now be considered. The solution for this model can be used to analyse the double porosity model and the patchy (partially) saturated model.

On the surface of the spherical inclusion having radius a, the elastic frame of the host and that of the inclusion are assumed to be in welded contact, so by continuity of displacement and the radial traction vectors we have (Deresiewicz & Skalak 1963) :

$$\mathbf{u}_i + \mathbf{u}_s = \mathbf{u}_f \quad (r = a), \tag{42}$$

$$\mathbf{t}_i + \mathbf{t}_s = \mathbf{t}_f \quad (r = a). \tag{43}$$

The continuity of the filtration velocity in the normal direction on a spherical surface is given by the expression,

$$\hat{\mathbf{r}} \cdot \mathbf{w}_i + \hat{\mathbf{r}} \cdot \mathbf{w}_s = \hat{\mathbf{r}} \cdot \mathbf{w}_f \quad (r = a), \tag{44}$$

where $\hat{\mathbf{r}}$ is unit vector in the outward (normal or radial) direction.

The interface Darcy's law governing fluid across the interface results is given by

$$\mathrm{i}\omega \hat{\mathbf{r}} \cdot \mathbf{w}_f = \kappa_{12}[p(\mathbf{u}_i, \mathbf{w}_i) + p(\mathbf{u}_s, \mathbf{w}_s) - p(\mathbf{u}_f, \mathbf{w}_f)] \quad (r = a). \tag{45}$$

Here, κ_{12} is called the interface permeability and is a function of the porosities and pore fluid mobilities of the two media. There is no theoretical or experimental work in the literature describing the interface permeability (Quiroga-Goode & Carcione 1997), but the limiting

cases are a sealed interface, $\kappa_{12} = 0$, which leads to $\hat{\mathbf{r}} \cdot \mathbf{w}_f = 0$ and an open interface, $k_s = \infty$, which leads to $p(\mathbf{u}_i, \mathbf{w}_i) + p(\mathbf{u}_s, \mathbf{w}_s) = p(\mathbf{u}_f, \mathbf{w}_f)$ on S.

Applying the orthogonality conditions of eqs (14) and (15) to the above boundary conditions, we get the following eight equations:

$$c_{3a1n}u_{3cn} - f_{3a1n}\bar{u}_{o\,3cn} = -a_{3a1n}\bar{u}_{3cn}, \tag{46}$$

$$c_{3a1n}t_{3cn} - f_{3a1n}\bar{t}_{o\,3cn} = -a_{3a1n}\bar{t}_{3cn}, \tag{47}$$

$$c_{1e1n}u_{1An} + c_{2e1n}u_{2An} + c_{4e1n}u_{4An} - f_{1e1n}\bar{u}_{o1An} - f_{2e1n}\bar{u}_{o2An} - f_{4e1n}\bar{u}_{o4An} = -a_{4e1n}\bar{u}_{4An}, \tag{48}$$

$$c_{1e1n}u_{1Bn} + c_{2e1n}u_{2Bn} + c_{4e1n}u_{4Bn} - f_{1e1n}\bar{u}_{o1Bn} - f_{2e1n}\bar{u}_{o2Bn} - f_{4e1n}\bar{u}_{o4Bn} = -a_{4e1n}\bar{u}_{4Bn}, \tag{49}$$

$$\begin{aligned} &c_{1e1n}(t_{1An} - p_{1An}) + c_{2e1n}(t_{2An} - p_{2An}) + c_{4e1n}t_{4An} - f_{1e1n}(\bar{t}_{o\,1An} - \bar{p}_{o\,1An}) \\ &\quad - f_{2e1n}(\bar{t}_{o\,2An} - \bar{p}_{o\,2An}) - f_{4e1n}\bar{t}_{o\,4An} = -a_{4e1n}\bar{t}_{4An}, \end{aligned} \tag{50}$$

$$c_{1e1n}t_{1Bn} + c_{2e1n}t_{2Bn} + c_{4e1n}t_{4Bn} - f_{1e1n}\bar{t}_{o1Bn} - f_{2e1n}\bar{t}_{o2Bn} - f_{4e1n}\bar{t}_{o4Bn} = -a_{4e1n}\bar{t}_{4Bn}, \tag{51}$$

$$\begin{aligned} &A_c c_{1e1n}u_{1An} + A_d c_{2e1n}u_{2An} + A_s c_{4e1n}u_{4An} - A_{oc}f_{1e1n}\bar{u}_{o1An} - A_{od}f_{2e1n}\bar{u}_{o2An} \\ &\quad - A_{os}f_{4e1n}\bar{u}_{o4An} = -A_s a_{4e1n}\bar{u}_{4An}, \end{aligned} \tag{52}$$

$$\begin{aligned} &c_{1e1n}\beta^{-1}p_{1An} + c_{2e1n}\beta^{-1}p_{2An} - f_{1e1n}\left(\beta_o^{-1}\bar{p}_{o1An} + \mathrm{i}\omega A_{oc}\bar{u}_{o1An}\kappa_{12}^{-1}\right) \\ &\quad - f_{2e1n}\left(\beta_o^{-1}\bar{p}_{o2An} + \mathrm{i}\omega A_{od}\bar{u}_{o2An}\kappa_{12}^{-1}\right) - f_{4e1n}\mathrm{i}\omega\bar{u}_{o4An}\kappa_{12}^{-1} = 0. \end{aligned} \tag{53}$$

For a given order n, there are eight unknown coefficients, c_{1e1n}, c_{2e1n}, c_{3a1n}, c_{4e1n} and f_{1e1n}, f_{2e1n}, f_{3a1n}, f_{4e1n}, which have to be determined from the above linear equation system. Two of the equations are independent and the remaining six linear algebraic equations need to be solved. It is very difficult to get the analytical solutions for the general porous case. However, it is not difficult to obtain numerical solutions.

The scattered wave (in the host material) is given by

$$\mathbf{u}_s = \sum_{n=1}^{\infty}(c_{1e1n}\psi_{1e1n} + c_{2e1n}\psi_{2e1n} + c_{3a1n}\psi_{3a1n} + c_{4e1n}\psi_{4e1n}), \tag{54}$$

$$\mathbf{w}_s = \sum_{n=1}^{\infty}(A_c c_{1e1n}\psi_{1e1n} + A_d c_{2e1n}\psi_{2e1n} + A_s c_{3a1n}\psi_{3a1n} + A_s c_{4e1n}\psi_{4e1n}). \tag{55}$$

6 THE VECTOR SCATTERING FUNCTION FOR SHEAR WAVES

If a plane S wave propagates through a poroelastic medium and impinges on a spherical inclusion made up of another poroelastic medium located at the original point, then by (54) the frame displacements of the scattered shear wave are

$$\mathbf{u}_s^s = \sum_{n=1}^{\infty}(c_{3a1n}\psi_{3a1n} + c_{4e1n}\psi_{4e1n}). \tag{56}$$

For the far-field situation ($k_s r \approx \infty$) and retaining terms of $O(r^{-1})$, we have

$$\psi_{3a1n} \approx [\exp(\mathrm{i}k_s r - \mathrm{i}\pi(n+1)/2/k_s r]\mathbf{C}_{a1n}, \tag{57}$$

$$\psi_{4e1n} \approx \mathrm{i}[\exp(\mathrm{i}k_s r - \mathrm{i}\pi(n+1)/2)/k_s r]\mathbf{B}_{a1n}. \tag{58}$$

Combining eqs (56)–(58), the scattered S waves in the far field can be rewritten as

$$\mathbf{u}_s^s = \mathbf{A}(\theta, \phi)\frac{\mathrm{e}^{\mathrm{i}k_s r}}{r}, \tag{59}$$

where the vector scattering function $\mathbf{A}(\theta, \phi)$ is given by

$$\mathbf{A}(\theta, \phi) = \sum_{n=1}^{\infty}\left\{\begin{array}{l} \left[c_{3a1n}\xi_n^{-1/2}(-\mathrm{i})^{n+1}\frac{1}{\sin\theta}\frac{\partial}{\partial\phi}Y_{1n}^a + c_{4e1n}\xi_n^{-1/2}(-\mathrm{i})^n\frac{\partial}{\partial\theta}Y_{1n}^e\right]\hat{\theta} \\ \\ -\left[c_{3a1n}\xi_n^{-1/2}(-\mathrm{i})^{n+1}\frac{\partial}{\partial\theta}Y_{1n}^a - c_{4e1n}\xi_n^{-1/2}(-\mathrm{i})^n\frac{1}{\sin\theta}\frac{\partial}{\partial\phi}Y_{1n}^e\right]\hat{\phi} \end{array}\right\}\frac{1}{k_s}. \tag{60}$$

From the definition of the spherical surface harmonic Y_{mn}^{σ} (see Appendix A), we find that

$$\left.\begin{array}{ll} \frac{1}{\sin\theta}\frac{\partial}{\partial\phi}Y_{1n}^a\Big|_{\substack{\theta=0\\ \phi=0}} = -\frac{n(n+1)}{2}; & \frac{\partial}{\partial\theta}Y_{1n}^a\Big|_{\substack{\theta=0\\ \phi=0}} = 0 \\ \frac{\partial}{\partial\theta}Y_{1n}^e\Big|_{\substack{\theta=0\\ \phi=0}} = -\frac{n(n+1)}{2}; & \frac{1}{\sin\theta}\frac{\partial}{\partial\phi}Y_{1n}^e\Big|_{\substack{\theta=0\\ \phi=0}} = 0 \end{array}\right\}. \tag{61}$$

Inserting eq. (61) into eq. (60) and using the relationship

$$\hat{\theta} = \cos\theta\,\cos\phi\hat{x} + \cos\theta\,\sin\phi\hat{y} - \sin\theta\hat{z}, \tag{62}$$

we have $\mathbf{A}(0,0) = A(0,0)\hat{\mathbf{x}}$ and

$$A(0,0) = -\sum_{n=1}^{\infty}(-\mathrm{i})^n\,(c_{4e1n} - \mathrm{i}c_{3a1n})\,\frac{\sqrt{2n+1}}{2\sqrt{2\pi}}\,\frac{1}{k_s}. \tag{63}$$

Appling the dynamic composite elastic medium theory (Kaelin & Johnson 1998), for the porous host having complex shear wavenumber k_s (eq. A.1) and randomly distributed identical inclusions of radius a and inclusion concentration (volume fraction) v, the effective non-self-consistent wavenumber k_{ns} can be written as

$$k_{\mathrm{ns}} = k_s + \frac{3vA(0,0)}{2k_s a^3}. \tag{64}$$

This equation can be used to calculate the phase velocity $c(\omega)$ and the specific inverse quality factor $Q(\omega)$ of the composite as follows:

$$c(\omega) = \mathrm{Re}^{-1}[1/V^*(\omega)], \tag{65}$$

$$\frac{1}{Q(\omega)} = \frac{\mathrm{Im}\left[V(\omega)^{*-2}\right]}{\mathrm{Re}\left[V(\omega)^{*-2}\right]}, \tag{66}$$

here $V_s(\omega)$ is the complex phase velocity $V_s(\omega) = \omega/k_{\mathrm{ns}}(\omega)$.

Before performing some numerical calculations and presenting results for a number of examples, we next show the analytical low frequency limits of the shear wave velocity of the double porosity model and the patchy saturation model. These analytic velocity results can be used to compare with our numerical values at low frequency and to check the validity of our two models.

7 THE LOW FREQUENCY LIMIT OF THE SHEAR WAVE PHASE VELOCITY FOR THE COMPOSITE

The effective shear elastic modulus μ_{e}^* and the effective bulk modulus K_{e}^* of an elastic composite with dilute concentration of elastic spheres can be uniquely determined by the volume fraction of spherical inclusions v (Christensen 1979).

$$\frac{\mu_{\mathrm{e}}^*}{\mu_{\mathrm{e}}} = 1 - \frac{15\,(1-\gamma_{\mathrm{e}})\left(1-\mu_{eo}/\mu_{\mathrm{e}}\right)v}{7-5\gamma_{\mathrm{e}}+2\,(4-5\gamma_{\mathrm{e}})\,\mu_{eo}/\mu_{\mathrm{e}}}. \tag{67}$$

Here μ_{e}, μ_{eo} are the shear and the bulk moduli of the host and the inclusion, respectively and γ_{e} is the Poisson's ratio of the host material. Under the assumption that the saturating fluid and the grain material are the same in both the host medium and the inclusion, Ciz *et al.* (2006) extend this formula into porous materials having porous inclusions of another material to determine the low frequency limit on the *P*-wave velocity. However, for the double porosity model at low frequencies, the averaged shear modulus μ_m^* is directly obtained by using eqs (67) and by substituting for the shear modulus of the porous host and the inclusion.

Thus, we can write the low frequency limit of the *S*-wave velocity as

$$c_s(0) = \sqrt{\frac{\mu_m^*}{(1-\beta^*)\rho_{\mathrm{s}} + \beta^*\rho_{\mathrm{f}}}}. \tag{68}$$

For shear waves in a patchy saturation model, the fluid in the host pores is different from that in the inclusions, but the drained moduli are the same in both the host and the inclusion. So, we have for the low frequency limit of the *S*-wave velocity in the patchy saturation model

$$c_s(0) = \sqrt{\frac{\mu_m}{(1-v)\,((1-\beta)\rho_{\mathrm{s}} + \beta\rho_{\mathrm{f}}) + v\,((1-\beta_o)\,\rho_{\mathrm{s}} + \beta_o\rho_{\mathrm{f}o})}}. \tag{69}$$

It is worth noting that the high-frequency velocity limit cannot be determined by Gassmann's fluid substitution, because Gassmann's results are static and actually only pertinent to low frequencies. Besides, at sufficiently high frequencies the shear modulus can in fact be related to the fluid's elastic properties (Berryman & Wang 2001). This issue is beyond the scope of our paper but it still needs further research.

8 NUMERICAL EXAMPLES

Ciz *et al.* (2006) apply Waterman–Truell multiple scattering theory and calculate the attenuation and phase velocity dispersion of the fast *P* wave in a saturated porous medium having a small volume concentration of randomly distributed spherical inclusions. To compare their results for *P* waves with ours for *S* waves, we use the same rock (mediums 1 and 2) and fluid parameters as they did, given in Table 1. But the porosity and permeability of medium 2 are chosen to have higher values. We choose the dynamic permeability model suggested by Johnson *et al.* (1987). So, tortuosity and pore volume-to-surface ratio can be expressed by the simple functions suggested by Sen *et al.* (1981) and Pride *et al.* (2004), respectively.

Table 1. Material properties of the sample rocks and fluids.

Parameter	Medium 1	Medium 2	Parameter	Water	Gas
K_s (N m^{-2})	3.3×10^{10}	3.3×10^{10}	K_f (N m^{-2})	2.25×10^9	0.0001×10^9
ρ_s (kg m^{-3})	2760	2760	ρ_f (kg m^{-3})	1000	1.2
K_m (N m^{-2})	1.26×10^{10}	1.26×10^8	η_f (kg m^{-1}s^{-1})	0.001	0.000018
μ_m (N m^{-2})	9.0×10^9	9.0×10^7	Dynamic permeability relationship		
κ_0 (m^2)	1.26×10^{-11}	1.26×10^{-8}	$\alpha_\infty = \beta^{-2/3}$ tortuosity		
β	0.16	0.32	$\Lambda = \sqrt{8\kappa_0\alpha_\infty/\beta}$ pore volume-to-surface ratio		

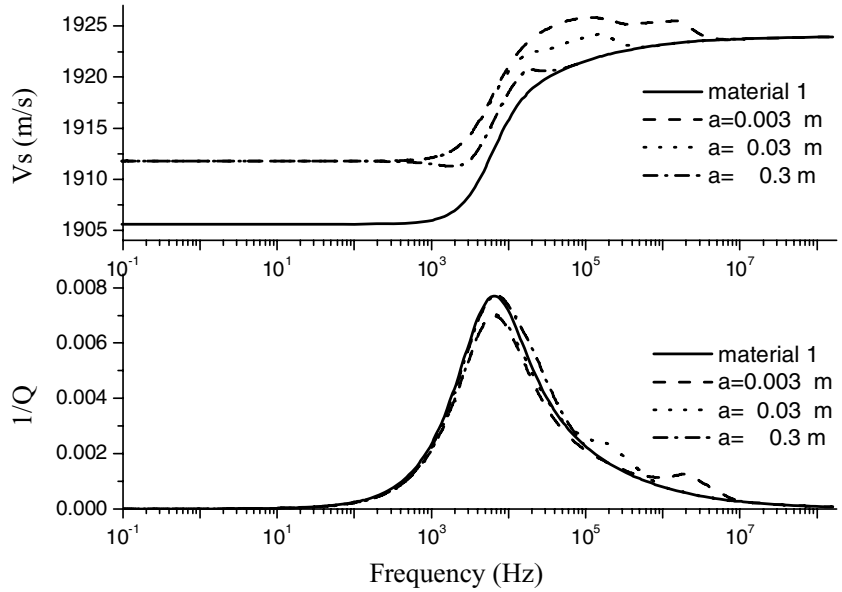

Figure 1. The dispersion curves of velocity (upper) and inverse quality factor (lower) of water-filled material 1 with identical gas-filled inclusions having a concentration of 10 per cent, and radii $a = 0.003$, 0.03 and 0.3 m, respectively.

By eq. (5), for homogeneous media 1 and 2 saturated with water the relaxation frequencies are (7900.1) and (29.1 Hz), respectively. By means of eqs (64), (65) and (66) we calculate the dispersion curves for various models.

Fig. 1 shows the dispersion curves of phase velocity (upper graph) and inverse quality factor (lower graph) for homogeneous water-filled material 1, and for the water-filled material 1 having identical gas-filled inclusions with a concentration of 10 per cent, and inclusion radii of $a = 0.003$, 0.03 and 0.3 m, respectively. The model with gas-filled inclusions is actually that of the patchy saturation model. The frequency dependence of the velocity and the attenuation basically has the same characteristics as those for the homogeneous material 1, although there are some differences. The inverse quality factor curves show that there are small attenuation peaks at frequencies at which the shear wavelength equals the size of the inclusion. On the other hand, the shear wave phase velocity curves show that at the low frequency limit, the shear velocity of the composite (1912 m s^{-1}) is higher than that of the host material (1905.6 m s^{-1}). This difference is caused entirely by the change of pore fluid density, which can be illustrated by using eq. (69) and getting the exact same result $c_s(0) = 1912$ m s^{-1}. At the higher frequency limit, the shear velocities of the composite equal the high frequency limit of the host porous medium. It is very clear that the patchy saturation situation with low gas concentration has almost no effect on the shear wave, which is very different from the case of an incident *P* wave. As is well known, even a tiny concentration of gas inclusions, like 3 per cent, will cause a significant attenuation of *P* waves over the seismic frequency range (White 1975; Dutta & Odé 1979a,b; Pride *et al.* 2004; Ciz *et al.* 2006). This peak occurs at a frequency at which the wavelength of the slow *P* wave equals the size of the inclusion. However, for case of shear wave incidence, there is no such attenuation mechanism.

Next, we consider the double porosity case, with homogeneous water-filled material 1, and water-filled material 1 having identical inclusions of water-filled material 2 at a concentration of 10 per cent, and inclusion radii $a = 0.003$, 0.03 and 0.3 m. Dispersion curves of phase velocity and attenuation are shown in Fig. 2. For each of the dispersion curves for the composites, the inverse quality factor shows significant attenuation peaks at frequencies where the shear wavelength approaches the size of the inclusion (these peaks shift to lower frequencies with larger inclusion size). Also, the phase velocity curve slopes upward at these frequencies. Superimposed on the curved sections are many sharp peaks, which represent resonances. A similar phenomenon of sharp peaks also occurs in the scattered cross-sections for elastic inclusions in an elastic host (Lim & Hackman 1990; Korneev & Johnson 1996). The sharp peaks in our dispersion curves are similar to the scattering in the pure elastic case. There is another small attenuation peak which occurs at the relaxation frequency of the host medium, which is apparently related to Biot's attenuation mechanism. At low frequencies where the shear wavelength is far larger than the size of the inclusion, the inverse quality factor is actually determined by that of the host material (solid line), and the shear velocity is

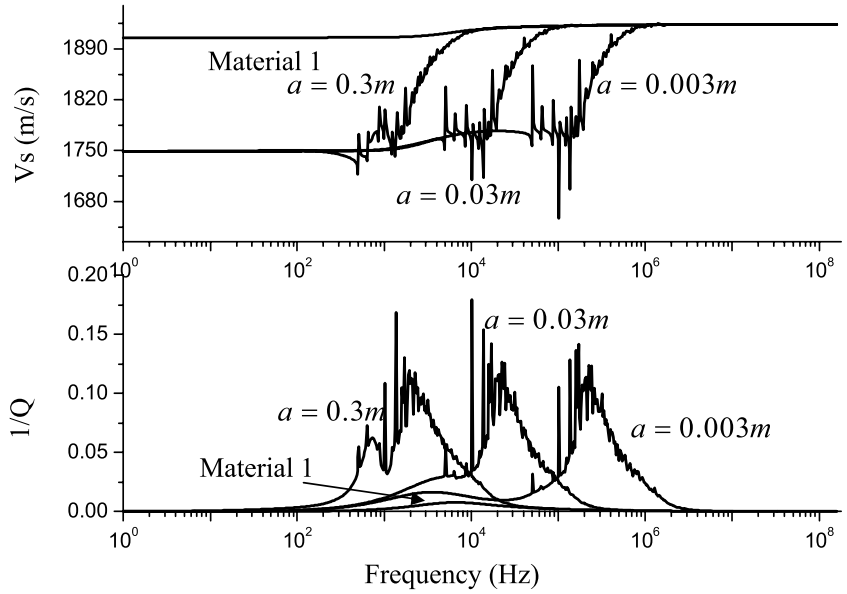

Figure 2. The dispersion curves of velocity (upper) and inverse quality factor attenuation (lower) of water-filled material 1 with identical inclusions of water-filled material 2 having a concentration of 10 per cent, and radii $a = 0.003$, 0.03 and 0.3 m, respectively.

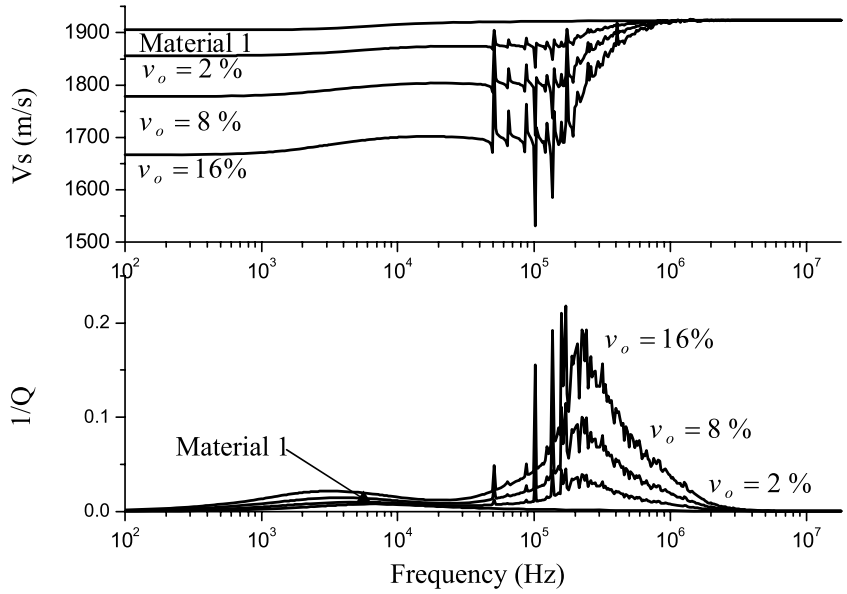

Figure 3. The dispersion curves of velocity (upper) and inverse quality factor attenuation (lower) of water-filled material 1 with identical inclusions of water-filled material 2 having a radius $a = 0.003$ m and inclusion concentrations of 2, 8 and 16 per cent, respectively.

1749 m s^{-1}. By eq. (68) we calculate a very similar low frequency limit of 1756 m s^{-1}. At high frequencies where the shear wavelength is far smaller than the size of the inclusion, the inverse quality factor $1/Q$ also equals that of the host material and the shear velocity approaches that of the host material (solid line).

Next, we look at the effect of inclusion concentration. Fig. 3 shows the dispersion curves (velocity and attenuation) for water-filled material 1 with identical inclusions of water-filled material 2 having a radius of $a = 0.03$ m, but for various inclusion concentrations of 2, 8 and 16 per cent. Again, this represents the double porosity model. The figure shows that larger volume fractions produce larger maximum values for the inverse quality factor $1/Q$ and lower values for the low frequency limit of the shear wave phase velocity. By eq. (68), we calculate the low frequency limit of shear velocity as 1871, 1760 and 1598 m s^{-1} for inclusion concentrations of 2, 8 and 16 per cent, respectively. From Fig. 3, it can be seen that our scattering model gives low frequency velocities of 1856, 1778 and 1667 m s^{-1} correspondingly. The relative discrepancies are 0.8, 1.0 and 4.1 per cent, respectively. The result is satisfying for small inclusion concentration and shows the validity of our equations and method. It shows that the non-self-consistent method, eq. (64), is not valid for large inclusion concentrations, which needs the self-consistent method. On the other hand, although the shear velocities of various volume fractions have different values at the low frequency

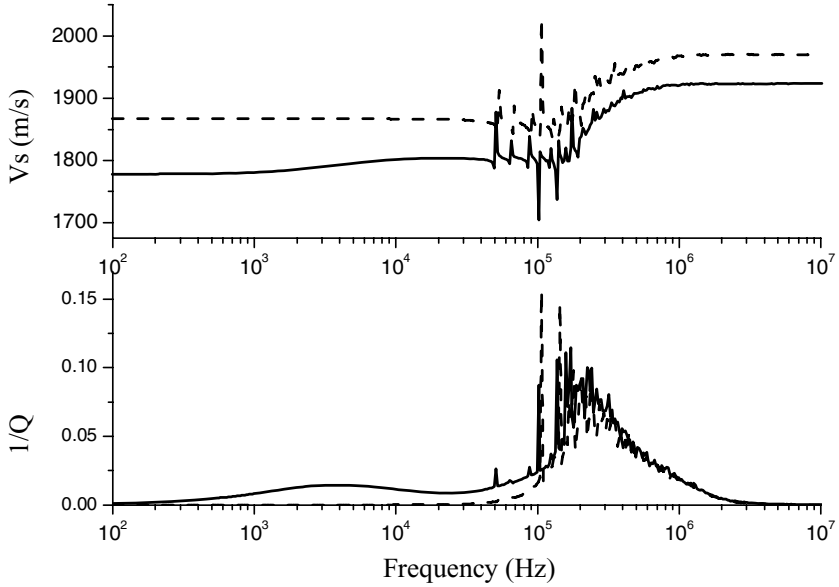

Figure 4. The dispersion curves of velocity (upper) and inverse quality factor (lower) of material 1 with identical inclusions of material 2 having a concentration of 8 per cent, and radius $a = 0.003$ m as double porosity cases. The solid lines denote pores filled with water and the dashed lines denote vacuumed pores.

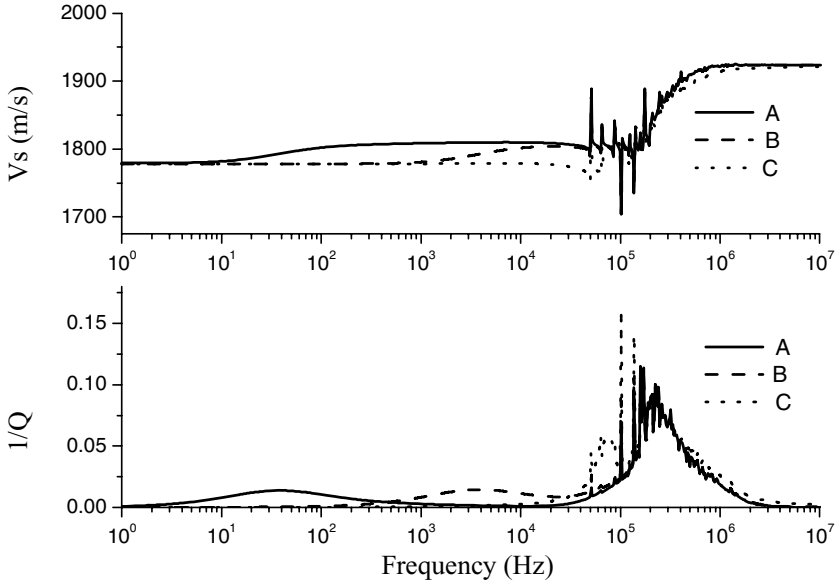

Figure 5. The dispersion curves of velocity (upper) and inverse quality factor (lower) for material 1 (different permeabilities) with identical inclusions of material 2 (different permeabilities) having a concentration of 8 per cent, and radius $a = 0.003$ m, as water-filled double porosity cases. The solid lines (marked with A) denote permeabilities of 9.5e−11 and 9.5e−9 m^2 for materials 1 and 2, respectively. The dashed lines (marked with B) denote the permeabilities of 9.5e−13 and 9.5e−10 m^2 for materials 1 and 2, respectively. The dotted lines (marked with C) denote the permeabilities of 9.5e−15 and 9.5e−11 m^2 for materials 1 and 2, respectively.

range, their values at high frequency approach the same high frequency limit of the host material (solid line). This result is consistent with that of elastic spherical scattering model developed by Kaelin & Jonhnson (1998).

In Fig. 4, the phase velocity and attenuation dispersion curves were computed for water-filled material 1 having identical inclusions of water-filled material 2, a radius of $a = 0.003$ m and an inclusion concentrations of 8 per cent. This double porosity case is presented as the solid line in both graphs. The other curves (shown as dashed lines) were calculated by the same model as for the solid line but setting the fluid density almost to zero (1.0×10^{-21} kg m^{-3}). In this case, the pore fluid will not affect the wavefield. If we notice the inverse quality factor curves and neglect the sharp resonance peaks, it is clear that the scattering attenuation peaks are very similar.

The final set of phase velocity and attenuation dispersion curves to examine the effect by fluid flow are presented in Fig. 5. They were computed for similar water-filled material as underlies Fig. 4, but for a range of permeabilities, from high to low. In our models, the permeability of the host dominates the effective dynamic permeability of the composite according to the approximation of the harmonic mean suggested by Pride *et al.* (2004). As shown in Fig. 5, as the permeability of the host material changes from

9.5×10^{-11} to 9.5×10^{-15} m^2, the scattering attenuation peaks occur over the same frequency range as in Fig. 4, with similar attenuation values. The attenuation peaks above 1.0×10^5 Hz are due to elastic scattering (*S* wave to *P* wave and *S* wave to *S* wave). At lower frequencies, the small amplitude smooth peaks are displaced towards the low frequency end with increasing permeability. This is clearly shown by eq. (5) which predicts an inverse proportionality between the Biot transition frequency and the permeability. By contrast, the characteristic frequency of S-P2 scattering should be proportional to permeability/viscosity. The computed results are in stark contrast to what one would expect if they are due to *S*-wave to slow *P*-wave scattering (Pride & Berryman 2003; Pride *et al.* 2004). We therefore conclude that such an attenuation mechanism is not important for spherical inclusions. This result verifies the fact that isotropic (spherical) geometries do not permit an applied pure shear to create changes in the fluid pressure of the constituents (Pride & Berryman 2003; Masson & Pride 2007). Of course, for ellipsoidal and other asymmetric (anisotropic) inclusion geometries this would not be the case.

9 CONCLUSIONS

The shear wave velocity and shear wave attenuation have been calculated for both the patchy saturation and the double porosity models with identical dilute inclusion concentrations.

It is well known that the maximum of the *P*-wave inverse quality factor occurs over the seismic frequency range for both the patchy saturation and the double porosity models. It occurs at a frequency at which the wavelength of the slow *P* wave equals the size of the inclusion. Since the diffusive (slow) *P* wave has very short wavelength, it causes significant attenuation at low frequency (Pride *et al.* 2004). However, the S-wave case is very different from that of the *P* wave.

From our calculations, it seems that although the fluid and the heterogeneity of the rock determine the shear wave velocity of the composite, the attenuation of the shear waves due to scattering is dominated by the heterogeneity of the rock, at least for spherical inclusion scattering. For the double porosity model, the softer inclusions with higher porosity cause significant shear wave attenuation at a wavelength which is approximately equal to the characteristic size of the inclusion. However, the shear attenuation can also be caused by local flow if the inclusions have some anisotropic geometry (see Pride & Berryman 2003; Pride *et al.* 2004). Therefore, both mechanisms mentioned above contribute to significant shear attenuation as observed in practice on both seismic and well-log records.

Although we do not provide the plots here, it is worth remarking that other calculations we have done show that neither the interface permeability (open or closed boundary) nor the permeability of the inclusions will actually affect the shear wave dispersion characteristics of the composite. This is also quite different from the result for *P*-wave incidence given by Ciz *et al.* (2006). They showed that the attenuation maximum shifts to higher frequencies with increasing permeability of inclusions.

Our results also show that the value of inverse quality factor maximum depends on the volume fraction of inclusions. For the patchy saturation model, the gas inclusions do not significantly affect the shear wave dispersion characteristic of the host medium, although small responses occur at frequencies at which the wavelength of the shear wave is approximately equal to the characteristic size of the inclusion. At low frequencies, because of the change in density, the shear velocity of the composite is different from the value of the host medium. Therefore, the difference between the two models for *S*-wave incidence provides a potential means to discriminate the type of medium.

Compared with analytic solutions for the low frequency limit of the shear velocity, the phase velocities in the low frequency range for our scattering model have relative discrepancies of less than 4.0 per cent. All calculated shear velocities of the composite with dilute inclusions will approach the high frequency limit of the host material. The result is satisfying and shows the validity of our equations and method.

In the future, we plan to derive the series or integral solution for shear wave scattering from porous ellipsoidal inclusions, which will then allow us to analyse the detailed processes of mode conversions by the calculation of energy cross-sections.

ACKNOWLEDGMENTS

This research was carried out under the support of the Australian Research Council. One of us (XL) wishes to acknowledge the financial support received from the University of Adelaide in the form of a postgraduate scholarship. The authors thank Dr M. Markov and an anonymous reviewer for their constructive reviews which helped improve the manuscript.

REFERENCES

Berryman, J.G., 1985. Scattering by a spherical inhomogeneity in a fluid-saturated porous medium, *J. Math. Phys.,* **26**(6), 1408–1419.

Berryman, J.G. & Milton, G.W., 1991. Exact results for generalized Gassmann's equations in composite porous media with two constituents, *Geophysics,* **56**(2), 1950–1960.

Berryman, J.G. & Wang, H.F., 2001. Dispersion in poroelastic systems, *Phys. Rev. E,* **64,** 011303, 1–16.

Biot, M.A., 1962. Mechanics of deformation and acoustic propagation in porous media, *J. Appl. Phys.,* **33**(4), 1482–1498.

Brown, R.J.S. & Korringa, J., 1975. On the dependence of the elastic properties of a porous rock on compressibility of the pore fluid, *Geophysics,* **40**(4), 608–616.

Christensen, R.M., 1979. *Mechanics of Composite Materials,* John Wiley & Sons, New York.

Ciz, R. & Gurevich, B., 2005. Amplitude of Biot's slow wave scattered by a spherical inclusion in a fluid-saturated poroelastic medium, *Geophys. J. Int.,* **160,** 991–1005.

Ciz R., Gurevich, B. & Markov, M., 2006. Seismic attenuation due to wave-induced fluid flow in a porous rock with spherical heterogeneities, *Geophys. J. Int.,* **165,** 957–968.

Deresiewicz, H. & Skalak, R., 1963. On uniqueness in dynamic poroelasticity, *Bull seism. Soc. Am.,* **53,** 783–788.

Dutta, N.C. & Odé, H., 1979a. Attenuation and dispersion of compressional waves in fluid-filled porous rocks with partial gas saturation (White model)-Part I: Biot theory, *Geophysics,* **44**(11), 1777–1788.

Dutta, N.C. & Odé, H., 1979b. Attenuation and dispersion of compressional waves in fluid-filled porous rocks with partial gas saturation (White model)-Part II: results, *Geophysics,* **44**(11), 1789–1805.

Einspruch, N.G., Witterholt, E.J. & Truell R., 1960. Scattering of a plane transverse wave by a spherical obstacle in an elastic medium, *J. Appl. Phys.,* **31**(5), 806–818.

Jones, T.D., 1986. Pore fluids and frequency-dependent wave propagation in rocks, *Geophysics,* **51**(10), 1939–1953.

Johnson, D.L., Koplik, J. & Dashen, R., 1987. Theory of dynamic permeability and tortuosity in fluid-saturated porous media, *J. Fluid Mech.,* **176,** 397–402.

Kargl, S.G & Lim, R., 1993. A transition-matrix formulation of scattering in homogeneous saturated porous media, *J. acoust. Soc. Am.,* **94**(3), 1527–1550.

Kaelin, B. & Jonhnson, L.R., 1998. Dynamic composite elastic medium theory, part II. three-dimensional media, *J. Appl. Phys.,* **84**(10), 5458–5468.

Korneev, V.A. & Johnson, L.R., 1993. Scattering of elastic waves by a spherical inclusion-I. Theory and numerical results, *Geophys. J. Int.,* **115,** 230–250.

Korneev, V.A. & Johnson, L.R., 1996. Scattering of P and S waves by a spherically symmetric inclusion, *Pure appl. Geophys.,* **147**(4), 675–718.

Lim, R. & Hackman, R.H., 1990. A parametric analysis of attenuation mechanisms in composites designed for echo reduction, *J. acoust. Soc. Am.,* **87**(3), 1076–1103.

Morochnik, V. & Bardet, J.P., 1996. Viscoelastic approximation of poroelastic media for wave scattering problems, *Soil Dyn. Earthquake Eng.,* **15,** 337–346.

Markov, M.G. & Levin, V.M., 2007. The role of surface tension in elastic wave scattering in an inhomogeneous poroelastic medium, *Waves Random Complex Media,* **17**(4), 615–626.

Masson, Y.J. & Pride, S.R., 2007. Poroelastic finite difference modeling of seismic attenuation and dispersion due to mesoscopic-scale heterogeneity, *J. geophys. Res.,* **112,** B03204, 1–16.

Morse, P.M. & Feshbach, H., 1953. *Methods of Theoretical Physics* (Part II) pp. 1759–1790, McGraw-Hill Book Company, INC. New York.

Müller, T.M. & Gurevich, B., 2005. A first-order statistical smoothing approximation for the coherent wave field in random porous media, *J. acoust. Soc. Am.,* **117**(4), 1796–1805.

Pride, S.R. & Berryman, J.G., 2003. Linear dynamics of double-porosity dual-permeability materials. I. Governing equations and acoustic attenuation, *Phys. Rev. E,* **68,** 036603, 1–10.

Pride, S.R., Berryman, J.G. & Harris, J.M., 2004. Seismic attenuation due to wave-induced flow, *J. geophys. Res.,* **109,** B01201, 1–19.

Quiroga-Goode, G. & Carcione, J.M., 1997. Heterogeneous modelling behaviour at an interface in porous media, *Comput. Geosci.,* **1,** 109–125.

Sen, P.N., Scala, C. & Cohen, M.H., 1981. A self-similar model for sedimentary rocks with application to the dielectric constant of fused glass beads, *Geophysics,* **46**(5), 781–795.

Waterman, P.C., 1976. Matrix theory of elastic wave scattering, *J. acoust. Soc. Am.,* **60**(3), 567–580.

White, J.E., 1975. Computed seismic speeds and attenuation in rocks with partial gas saturation, *Geophysics,* **40**(2), 224–232.

Zimmerman, C. & Stern, M., 1993. Scattering of plane compressional waves by spherical inclusions in a poroelastic medium, *J. acoust. Soc. Am.,* **94**(1), 527–536.

Zimmerman, C. & Stern, M., 1994. Analytical solutions for harmonic wave propagation in poroelastic media, *J. Eng. Mech.,* **120**(10), 2154–2178.

APPENDIX A: THE COMPLEX WAVENUMBERS AND RELATIVE FLUID DISPLACEMENT COEFFICIENTS

$$k_s^2 = \frac{\omega^2}{\mu}\left(\rho - \frac{\rho_{\mathrm{f}}^2}{q(\omega)}\right), \tag{A1}$$

$$k_d^2 = \omega^2 \frac{c_1\delta_{22} - c_3\delta_{12}}{c_1c_4 - c_2c_3}, \tag{A2}$$

$$k_c^2 = \omega^2 \frac{c_2\delta_{21} - c_4\delta_{12}}{c_3c_2 - c_1c_4}, \tag{A3}$$

$$\left.\begin{array}{ll} \delta_{11} = \rho\delta_d + \rho_{\mathrm{f}} & c_1 = (\lambda_{\mathrm{c}} + 2\mu)\delta_d + \alpha M \\ \delta_{12} = \rho\delta_c + \rho_{\mathrm{f}} & c_2 = (\lambda_{\mathrm{c}} + 2\mu)\delta_c + \alpha M \\ \delta_{21} = \rho_{\mathrm{f}}\delta_d + q(\omega) & c_3 = \alpha M\delta_d + M \\ \delta_{22} = \rho_{\mathrm{f}}\delta_c + q(\omega) & c_4 = \alpha M\delta_c + M \end{array}\right\}, \tag{A4}$$

$$\delta_c = \frac{-B - \sqrt{B^2 - 4AC}}{2A} \quad \text{and} \quad \delta_d = \frac{-B + \sqrt{B^2 - 4AC}}{2A}, \tag{A5}$$

$$\left.\begin{array}{l} A = \rho\alpha M - \rho_{\mathrm{f}}(\lambda_{\mathrm{c}} + 2\mu) \\ B = \rho M - q(\omega)(\lambda_{\mathrm{c}} + 2\mu) \\ C = -q(\omega)\alpha M + M\rho_{\mathrm{f}} \end{array}\right\} \tag{A6}$$

$$A_s = -\frac{\rho_{\mathrm{f}}}{q(\omega)} \quad A_d = \delta_c^{-1} \quad \text{and} \quad A_c = \delta_d^{-1}. \tag{A7}$$

APPENDIX B: FORM OF THE VECTOR SPHERICAL HARMONICS

$$\mathbf{A}_{\sigma mn}(\theta, \phi) = \hat{\mathbf{r}} Y_{mn}^{\sigma}(\theta, \phi), \tag{B1}$$

$$\mathbf{B}_{\sigma mn}(\theta,\phi)=\xi_n^{-1/2}\frac{\partial}{\partial\theta}Y^{\sigma}_{mn}(\theta,\phi)\hat{\theta}+\xi_n^{-1/2}\frac{1}{\sin\,\theta}\frac{\partial}{\partial\phi}Y^{\sigma}_{mn}(\theta,\phi)\hat{\phi}, \tag{B2}$$

$$\mathbf{C}_{\sigma mn}(\theta,\phi)=\xi_n^{-1/2}\frac{1}{\sin\,\theta}\frac{\partial}{\partial\phi}Y^{\sigma}_{mn}(\theta,\phi)\hat{\theta}-\xi_n^{-1/2}\frac{\partial}{\partial\theta}Y^{\sigma}_{mn}(\theta,\phi)\hat{\phi}, \tag{B3}$$

where $\hat{\mathbf{r}}$, $\hat{\theta}$ and $\hat{\phi}$ are unit vectors in spherical coordinates and

$$Y^{\sigma}_{mn}(\theta,\phi)=\left(\frac{\varepsilon_m(2n+1)(n-m)!}{4\pi(n+m)!}\right)^{1/2}P_n^m(\cos\theta)\begin{pmatrix}\cos\,m\phi, & \sigma=e\\ \sin\,m\phi, & \sigma=a\end{pmatrix}. \tag{B4}$$

The factor ε_m is defined by $\varepsilon_{m=0}=1$ and $\varepsilon_{m>0}=2$. When $m=1$, we have

$$Y^{\sigma}_{1n}(\theta,\phi)=\left(\frac{2n+1}{2\pi n(n+1)}\right)^{1/2}P_n^1(\cos\theta)\begin{pmatrix}\cos\,\phi, & \sigma=e\\ \sin\,\phi, & \sigma=a\end{pmatrix}. \tag{B5}$$

APPENDIX C: COEFFICIENTS OF THE VECTOR SPHERICAL HARMONICS

The coefficients appearing in eqs (3.7)–(3.17) are given by

$u_{1An}=F_c^{-1}h_n'(k_cr)$, $\quad u_{1Bn}=F_c^{-1}\xi_n^{1/2}[h_n(k_cr)/k_cr]$, $\quad u_{2An}=F_d^{-1}h_n'(k_dr)$,

$u_{2Bn}=F_d^{-1}\xi_n^{1/2}[h_n(k_dr)/k_dr]$, $\quad u_{3Cn}=h_n(k_sr)$, $\quad u_{4An}=\xi_n^{1/2}[h_n(k_sr)/k_sr]$ and

$u_{4Bn}=[h_n'(k_sr)+h_n(k_sr)/k_sr]$,

$$t_{1An}=2\mu k_cF_c^{-1}\left[\left(\xi_n-\frac{(P+QA_c)(k_cr)^2}{2\mu}\right)\frac{h_n(k_cr)}{(k_cr)^2}-\frac{2h_n'(k_cr)}{k_cr}\right],$$

$$t_{1Bn}=2\mu k_cF_c^{-1}\xi_n^{1/2}\left[\frac{h_n'(k_cr)}{k_cr}-\frac{h_n(k_cr)}{(k_cr)^2}\right],$$

$$t_{2An}=2\mu k_dF_d^{-1}\left[\left(\xi_n-\frac{(P+QA_d)(k_dr)^2}{2\mu}\right)\frac{h_n(k_dr)}{(k_dr)^2}-\frac{2h_n'(k_dr)}{k_dr}\right],$$

$$t_{2Bn}=2\mu k_dF_d^{-1}\xi_n^{1/2}\left[\frac{h_n'(k_dr)}{k_dr}-\frac{h_n(k_dr)}{(k_dr)^2}\right],$$

$$t_{3Cn}=\mu k_s\left[h_n'(k_sr)-\frac{h_n(k_sr)}{k_sr}\right],$$

$$t_{4An}=2\mu k_s\xi_n^{1/2}\left[\frac{h_n'(k_sr)}{k_sr}-\frac{h_n(k_sr)}{(k_sr)^2}\right],$$

$$t_{4Bn}=2\mu k_s\left[\left(\xi_n-1-\frac{(k_sr)^2}{2}\right)\frac{h_n(k_sr)}{(k_sr)^2}-\frac{h_n'(k_sr)}{k_sr}\right],$$

$$p_{1An}=k_cF_c^{-1}(Q+RA_c)\,h_n(k_cr),$$

$$p_{2An}=k_dF_d^{-1}(Q+RA_d)\,h_n(k_dr).$$